DOI: 10.1002/anie.200802867

Quantum Dots

Synthetic Scheme for High-Quality InAs Nanocrystals Based on Self-Focusing and One-Pot Synthesis of InAs-Based Core–Shell Nanocrystals**

*Renguo Xie and Xiaogang Peng**

Synthetic chemistry of colloidal semiconductor nanocrystals (quantum dots) has attracted substantial interest in recent years. A key concept for formation of nearly monodisperse nanocrystals, namely focusing of size distribution,[1] was discovered upon studying the growth of high-quality CdSe quantum dots. This concept implies that if all nuclei are formed in the beginning and stop growing promptly, as triggered by a decrease in monomer concentration or lower reaction temperature, the subsequent growth process will focus the size distribution of the nanocrystals. This is so because the smaller nanocrystals should grow faster by consuming the residual dissolved monomer if the monomer concentration is higher than the solubility of all nanocrystals in the solution. The key feature of this method is the constant particle concentration during particle growth. Computer simulations revealed that the size distribution of nanocrystals could also be focused through Ostwald ripening, but the final size distribution would still be quite broad.[2] Herein, we demonstrate that InAs nanocrystals with well-controlled size and size distribution can be formed by a special ripening process, called self-focusing of size distribution (in short, self-focusing).[3,4] Different from traditional focusing of size distribution, the particle concentration decreases drastically in the growth process, and the monomers are driven from small nanocrystals to larger ones by interparticle diffusion, owing to solubility gradients between neighboring nanoparticles.[3] An additional feature is that the temperature for self-focusing is much higher than the nucleation temperature. To our knowledge, this is the first time that interparticle diffusion and self-focusing have been purposely employed for the controlled synthesis of nanocrystals.

High-quality InAs nanocrystals are likely the best candidates for quantum-dot emitters in the near infrared (NIR) window (700–1400 nm) among II–VI, III–V, and IV–VI semiconductor nanocrystals[5] if Class A elements, such as Cd, Hg, and Pb, are excluded. NIR emitters are important for both in vivo biomedical imaging[5–11] and telecommunications.[12] Because of the extreme sensitivity of InAs nanocrystals to air oxidation and the large exciton size, such NIR emitters should be epitaxially coated with other types of wide-band-gap semiconductors. Given the narrow bulk band gap of InAs (ca. 0.4 eV), core nanocrystals of this material for building core–shell nanocrystals that emit in NIR range should be smaller than roughly 3 nm.

Experimental details are provided as Supporting Information; a brief procedure is as follows. A mixture of indium stearate (0.4 mM), trioctylphosphine (0.5 mL), and octadecene (ODE, 3.5 mL) was heated to 150 °C under an argon flow. $As(Si(CH_3)_3)_3$ solution made in the glove box (ca. 0.1 mmol) was introduced into the reaction solution, and the reaction was held at 150 °C for a couple of minutes to convert all arsenic precursors to InAs nanoclusters. Subsequently, the reaction solution was heated to a desired temperature (up to 300 °C) for the growth of InAs nanocrystals with different sizes.

Synthesis of III–V quantum dots has been a challenging task,[1,5,12,13–21] and their development lags substantially behind that of their II–VI and IV–VI analogues.[22] The synthetic procedure described above was developed after our failed efforts to extend the recently developed synthetic scheme for InP nanocrystals[23] to InAs. Comparing InAs quantum dots with those made of InP, initial efforts revealed that the more reactive precursor ($As(Si(CH_3)_3)_3$ vs. $P(Si(CH_3)_3)_3$) always generated small nanoclusters (less than 1 nm) with a fixed spectrum using the same synthetic scheme as for InP (see the Supporting Information, Figure 1S). Elimination of the activation reagent (fatty amine) and addition of free fatty acids as inhibitors[22] still yielded magic-sized nanoclusters with two distinguishable and persistent absorption peaks[24] at 420 and 460 nm (the first spectrum in all plots in the left panel of Figure 1). Interestingly, the particle concentration was found to decrease by adding free fatty acid to the reaction system. When the fatty acid concentration was high, some grayish deposition (likely arsenic metal) on the dry part of the reaction flask was observed. Similarly, at high reaction temperatures, the intensity of the two peaks at 420 and 460 nm decreased as the reaction temperature increased. Furthermore, the particle concentration did not increase by using excess indium stearate.

Because of the high reactivity of the arsenic precursor, almost immediately after the reaction started, all molecular arsenic species would be consumed by either forming InAs nanoclusters or being decomposed (decomposition was accelerated by the presence of fatty acids and by high temperature). The direct consequence of this conclusion is

[*] Dr. R. G. Xie, Prof. X. G. Peng
Department of Chemistry and Biochemistry
University of Arkansas, Fayetteville, AR 72701 (USA)
Fax: (+1) 479-575-4049
E-mail: xpeng@uark.edu

[**] X. Peng thanks the NSF and NIH for funding support, and we thank Dr. M. Benamara for HRTEM measurements.

Supporting information for this article is available on the WWW under http://dx.doi.org/10.1002/anie.200802867.

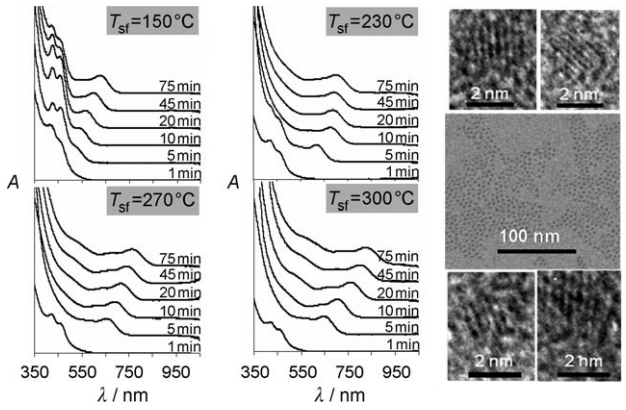

Figure 1. Left panel: Growth of InAs nanocrystals at different self-focusing temperatures (T_{sf}). Right panel: Low-resolution and corresponding high-resolution TEM images of InAs nanocrystals.

that, without residual monomer after the nucleation process, continuous growth of InAs nanocrystals through the incorporation of dissolved monomer would not be possible. This situation automatically excluded the possibility to apply the commonly used focusing of size distribution technique[1] for this system.

However, this reaction system seemed to be suited for applying the newly discovered self-focusing of size distribution through interparticle diffusion.[3,4] The high particle concentration in solution (see below) should enable the needed overlap of the diffusion spheres of adjacent particles. As a result, a solubility gradient between adjacent nanocrystals should drive monomers close to the surface of a small nanocrystal or nanocluster to a larger one within the overlapped diffusion spheres. If this mechanism is at work, the complete dissolution of small particles and relative slow growth of large ones (owing to the cubic dependence of the volume of a crystal on its diameter) should result in a nearly monodisperse ensemble. As pointed out previously,[3,4] the rapid dissolution of the small particles is the key to complete dissolution of these sacrificial particles within the reaction timeframe, to avoid a log-normal size distribution for a typical Ostwald ripening process. The extremely small sizes of the nanoclusters and nanocrystals in this system mean that a large solubility gradient can easily be realized, owing to the exponential increase of the particles' solubility according to the Gibbs–Thompson equation.[25] Although the persistent peaks indicate that magic-sized nanoclusters are the main component in the solution, the broad absorption spectra of the initial solutions (Figure 1) imply that there was a size distribution around the magic-sized particles.

For the reactions discussed below, the InAs nanoclusters were formed by adding $As(Si(CH_3)_3)_3$ precursor into the reaction system at 150 °C. A lower temperature, for example 70 °C, would result in slower formation of the InAs nanoclusters without substantially affecting the subsequent self-focusing. After the absorbance at the peak positions of the nanoclusters reached a constant value, the reaction system was heated up to a designated self-focusing temperature (T_{sf}). As shown in Figure 1 (left), upon heating the nanoclusters became unstable, and the relatively large InAs nanocrystals grew, as judged by the temporal evolution of the absorption spectrum for each case. The rate of disappearance of the absorption peaks at 420 and 460 nm from the initial InAs nanoclusters was found to depend strongly on T_{sf}. The initial nanoclusters disappeared completely upon heating at a T_{sf} higher than 180 °C and partially for T_{sf} in the range 130–180 °C (Figure 1). When T_{sf} was lower than 120 °C, neither dissolution of the initial nanoclusters nor formation of large InAs nanocrystals was observed.

The well-resolved spectral features in the resulting nanocrystals imply a focused size distribution, which is consistent with the transmission electron microscopy (TEM) observations for the larger InAs nanocrystals (Figure 1, right panel). The final size of the InAs nanocrystals obtained by self-focusing was found to be determined by the T_{sf} (Figure 1, left and middle panel).

The self-focusing nature of nanocrystal growth shown in Figure 1 was verified by quantitative analysis. For two different focusing temperatures, Figure 2 illustrates the temporal

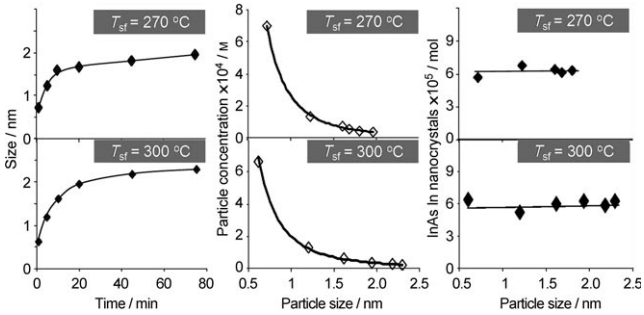

Figure 2. Temporal evolution of size, particle concentration, and InAs yield for two reactions with different self-focusing temperatures.

evolution of the average size (left), particle concentration (middle), and the yield of InAs molecular units in the form of nanoclusters or nanocrystals (right). For clarity, the latter two are plotted against the size of the particles. Upon rapid growth of the nanocrystals (Figure 2, left), the particle concentration decreased sharply (Figure 2, middle) with the InAs unit yield in the form of nanoclusters or nanocrystals being constant (Figure 2, right). For example, when T_{sf} = 300 °C, the initial particle concentration was 6.6×10^{-4} M, and the InAs yield in molecular units was almost unity. The final particle concentration decreased by 30 times from the initial value (Figure 2, middle bottom), which is equivalent to 97 % of the initial nanoclusters being completely dissolved. These results are consistent with the features of self-focusing. Furthermore, the average particle separation calculated for the initial stage was only about 14 nm. Even without considering thermal motion of the particles, this distance is already small in comparison to the size of the diffusion spheres, which means that the required short distance for interparticle diffusion was, indeed, realized.[3] The temperature dependence of the final size of the nanocrystals (Figure 1, left and middle panel) is probably caused by two factors. In general, the diffusion rate is proportional to the temperature increase,

and a higher temperature should enhance the probability for the close approach of the nanocrystals.

For the targeted emission colors, the InAs nanocrystals should be in the size range of 1–3 nm to cover the desired NIR emission window. These extremely small sizes, together with the unstable nature of InAs nanocrystals, make these particles unsuitable for direct imaging using TEM.[15] In fact, the size determination of semiconductor nanocrystals smaller than approximately 2 nm has been generally problematic. We developed a method to solve this problem by growing high-quality core–shell nanocrystals and analyzing the core–shell structure using TEM and elemental analysis with atomic absorption (AA). CdSe was chosen as the shell material for two reasons: a perfect crystal lattice match[12] and different composition in both cation and anion from InAs.

InAs/CdSe core–shell nanocrystals were grown at 180–190 °C using a one-pot successive ionic layer adsorption and reaction (SILAR) technique.[26] Upon shell growth, the size of the nanocrystals increased (Figure 3, left panel), and the UV/Vis and photoluminescence (PL) spectra of the resulting core–shell nanocrystals shifted substantially towards red (Figure 3 d). Provided the small size of the core InAs nanocrystals, this substantial red shift should be considered as solid evidence of CdSe shell growth, as opposed to formation of an alloy of the core and shell.[27] The PL quantum yield (QY) of the core–shell nanocrystals was found to increase dramatically from below 1 % to as high as 90 % (see the Supporting Information, Figure 2S). The full width at half maximum of the PL peak of the core–shell nanocrystal could be maintained at the value of the InAs core nanocrystals (about 70 nm on average for the example in Figure 3 d as opposed to over 120 nm reported for similar structures emitting at similar wavelengths).[12] Moreover, the resulting core–shell nanocrystals were found to be stable and emissive in air and in aqueous solution after surface-ligand replacement with hydrophilic thiols (see the Supporting Information, Figure 3S). High-resolution TEM (HRTEM) images and electron diffraction patterns (see the Supporting Information, Figure 4S) revealed that the shells of the nanocrystals were epitaxially grown in the zinc blende structure of the InAs core. Although core–shell growth is not the main focus of this work, it should be pointed out that the one-pot approach also worked for the other types of core–shell nanocrystals, such as InAs/InP and InAs/ZnSe (Figure 3 f).

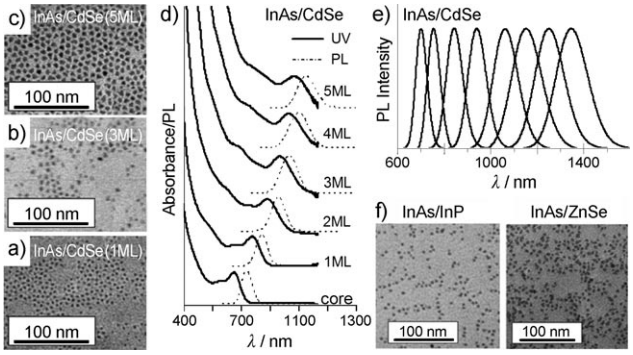

Figure 3. Characterization of InAs-based core–shell nanocrystals. a–c) TEM images of InAS/CdSe nanocrystals. ML = monolayer. d) UV/Vis absorption and photoluminescence spectra of nanocrystals with shells of different thickness. e) Photoluminescence of different nanocrystals; the emission can be tuned in the IR region. f) TEM images of InAs/InP and InAs/ZnSe core–shell nanocrystals.

The average size of the large and stable InAs/CdSe core–shell nanocrystals was readily determined by TEM (Figure 3 and Figure 3S in the Supporting Information). Such core–shell nanocrystals were subjected to digestion for elemental analysis, which determined the atomic ratio between different elements. Because CdSe was epitaxially grown onto the InAs core nanocrystals and the two semiconductors have the same lattice constants,[12] the volume ratio of the core and shell should be equal to the Cd/In atomic ratio. Thus, the size of the core could be readily obtained by assuming a spherical shape for both core and core–shell nanocrystals. The table in Figure 4 (top) summarizes the sizes of several representative core–shell nanocrystals measured by TEM, the Cd/Se atomic ratio, the Cd/In atomic ratio, and the core size calculated from the TEM and atomic ratio results. The Cd/Se and In/As ratios of the core–shell nanocrystals were both monitored to further verify the purity of the CdSe shell, and both were very close to the ideal 1:1 ratio (see Cd/Se ratios as examples). This finding indicates that, after excluding alloy structures as discussed above, the shell should be pure CdSe.

The sizes of InAs nanocrystals determined using the method described above are plotted along with the literature values.[1] Good agreement in the overlapping size range is evident in Figure 4 a. A numerical fitting of all data was obtained.

Size of InAs/CdSe (nm)	3.2	3.1	3.9	5.5
Cd/Se atomic ratio	1:0.94	1:1.07	1:0.96	1:0.97
Cd/In atomic ratio	1:0.082	1:0.24	1:0.33	1:0.1
Calculated size of InAs (nm)	1.32	1.80	2.18	2.52

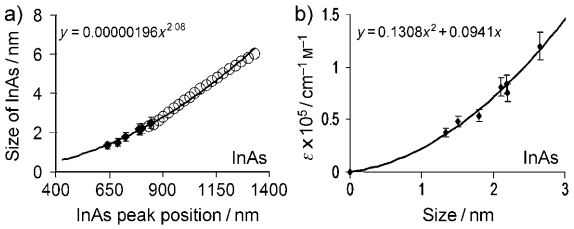

Figure 4. TEM and AA results for several InAs/CdSe core–shell samples (top). a) Size of InAs nanocrystals verses their first exitonic absorption peak (○ literature, ◆ this work). b) The molar extinction coefficient (ε) of InAs nanocrystals. The solid lines in (a) and (b) are numerical fittings.

The structural information discussed above was further used for determining the molar extinction coefficient of the InAs nanocrystals (per mole of particles, Figure 4 b). The sizing curve and the molar extinction coefficients shown in Figure 4 were used for processing the experimental data in Figure 2.

In summary, InAs nanocrystals for NIR emission were synthesized through self-focusing of size distribution. The new strategy introduced herein yielded nearly monodisperse InAs nanocrystals with different sizes in quantitative yield by

increasing the growth temperature, and the final size of the resulting nanocrystals was controlled by the temperature. The synthetic strategy was found to be suited for the one-pot growth of core–shell nanocrystals with bright (up to 90% PL QY), stable, and narrow photoluminescence in the optical window desired for in vivo biomedical imaging and telecommunications (700–1400 nm). Because the InAs nanocrystals were grown under conditions close to the ripening threshold, the surface of the nanocrystals could be better controlled, which probably contributed to the formation of nanocrystals with outstanding emission properties. The extremely small sizes of the InAs nanocrystals were shown to be measurable using a combined TEM–AA method and InAs/CdSe core–shell nanocrystals.

Experimental Section

A typical synthetic reaction for synthesis of InAs core dots is provided in the text. One-pot synthesis of core–shell QDs based on the InAs core is provided as Supporting Information. Carbon-coated copper grids were dipped in hexanes or toluene solutions with the nanocrystals to deposit the nanocrystals onto the carbon film. The low-resolution transmission electron microscopy (TEM) images were taken on a JEOL 100CX transmission electron microscope with an acceleration voltage of 100 kV. High-resolution TEM (HRTEM) pictures were taken using a Taitan microscope with an acceleration voltage of 300 KV. Absorption spectra were measured on a HP 8453 diode array spectrophotometer. Photoluminescence (PL) was measured on a Spex Fluorolog 3–111 using a PMT detector for spectra between 400 and 850 nm and a liquid-nitrogen-cooled InGaAs photodiode detector for emission in the NIR (700–1500 nm). PL quantum yields (QYs) of the samples were determined using organic dyes with known quantum yields as standards. Details for atomic absorption (AA) measurements are provided in the Supporting Information.

Received: June 16, 2008
Published online: August 29, 2008

Keywords: fluorescence · nanocrystals · quantum yield · semiconductors

[1] X. Peng, J. Wickham, A. P. Alivisatos, *J. Am. Chem. Soc.* **1998**, *120*, 5343.
[2] D. Talapin, A. Rogach, M. Haase, H. Weller, *J. Phys. Chem. B* **2001**, *105*, 12274.
[3] J. Thessing, J. Qian, H. Chen, N. Pradhan, X. Peng, *J. Am. Chem. Soc.* **2007**, *129*, 2736.
[4] Y. Chen, E. Johnson, X. Peng, *J. Am. Chem. Soc.* **2007**, *129*, 10937.
[5] J. P. Zimmer, S.-W. Kim, S. Ohnishi, E. Tanaka, J. V. Frangioni, M. G. Bawendi, *J. Am. Chem. Soc.* **2006**, *128*, 2526.
[6] B. Dubertret, P. Skourides, D. J. Norris, V. Noireaux, A. H. Brivanlou, A. Libchaber, *Science* **2002**, *298*, 1759.
[7] D. R. Larson, W. R. Zipfel, R. M. Williams, S. W. Clark, M. P. Bruchez, F. W. Wise, W. W. Webb, *Science* **2003**, *300*, 1434.
[8] X. Gao, Y. Cui, R. M. Levenson, L. W. K. Chung, S. Nie, *Nat. Biotechnol.* **2004**, *22*, 969.
[9] S. Kim, Y. T. Lim, E. G. Soltesz, A. M. De Grand, J. Lee, A. Nakayama, J. A. Parker, T. Mihaljevic, R. G. Laurence, D. M. Dor, L. H. Cohn, M. G. Bawendi, J. V. Frangioni, *Nat. Biotechnol.* **2004**, *22*, 93.
[10] X. Michalet, F. F. Pinaud, L. A. Bentolila, J. M. Tsay, S. Doose, J. J. Li, G. Sundaresan, A. M. Wu, S. S. Gambhir, S. Weiss, *Science* **2005**, *307*, 538.
[11] W. Liu, H. S. Choi, J. P. Zimmer, E. Tanaka, J. V. Frangioni, M. Bawendi, *J. Am. Chem. Soc.* **2007**, *129*, 14530.
[12] A. Aharoni, T. Mokari, I. Popov, U. Banin, *J. Am. Chem. Soc.* **2006**, *128*, 257.
[13] O. I. Micic, J. R. Sprague, C. J. Curtis, K. M. Jones, J. L. Machol, A. J. Nozik, H. Giessen, B. Fluegel, G. Mohs, N. Peyghambarian, *J. Phys. Chem.* **1995**, *99*, 7754.
[14] A. A. Guzelian, J. E. B. Katari, A. V. Kadavanich, U. Banin, K. Hamad, E. Juban, A. P. Alivisatos, R. H. Wolters, C. C. Arnold, J. R. Heath, *J. Phys. Chem.* **1996**, *100*, 7212.
[15] A. A. Guzelian, U. Banin, A. V. Kadavanich, X. Peng, A. P. Alivisatos, *Appl. Phys. Lett.* **1996**, *69*, 1432.
[16] Y.-W. Cao, U. Banin, *Angew. Chem.* **1999**, *111*, 3913–3916; *Angew. Chem. Int. Ed. Engl.* **1999**, *38*, 3692–3694.
[17] D. Battaglia, X. Peng, *Nano Lett.* **2002**, *2*, 1027.
[18] D. V. Talapin, A. L. Rogach, E. V. Shevchenko, A. Kornowski, M. Haase, H. Weller, *J. Am. Chem. Soc.* **2002**, *124*, 5782.
[19] D. V. Talapin, N. Gaponik, H. Borchert, A. L. Rogach, M. Haase, H. Weller, *J. Phys. Chem. B* **2002**, *106*, 12659.
[20] P. Yu, C. Beard Matthew, J. Ellingson Randy, S. Ferrere, C. Curtis, J. Drexler, F. Luiszer, J. Nozik Arthur, *J. Phys. Chem. B* **2005**, *109*, 7084.
[21] D. W. Lucey, D. J. MacRae, M. Furis, Y. Sahoo, A. N. Cartwright, P. N. Prasad, *Chem. Mater.* **2005**, *17*, 3754.
[22] X. Peng, J. Thessing, *Struct. Bonding (Berlin)* **2005**, *118*, 79.
[23] R. Xie, D. Battaglia, X. Peng, *J. Am. Chem. Soc.* **2007**, *129*, 15432.
[24] Z. A. Peng, X. Peng, *J. Am. Chem. Soc.* **2002**, *124*, 3343.
[25] J. W. Mullin, *Crystallization*, third ed., Butterworth-Heinemann, Oxford, **1997**.
[26] J. J. Li, Y. A. Wang, W. Guo, J. C. Keay, T. D. Mishima, M. B. Johnson, X. Peng, *J. Am. Chem. Soc.* **2003**, *125*, 12567.
[27] X. Peng, M. C. Schlamp, A. V. Kadavanich, A. P. Alivisatos, *J. Am. Chem. Soc.* **1997**, *119*, 7019.

